Modelling the influence of steel structure compartment geometry on travelling fires

Modelling the influence of steel structure compartment geometry on travelling fires

Author 1
- Marion Charlier, Research engineer
- ArcelorMittal Global R&D, Esch/Alzette, Luxembourg
- https://orcid.org/0000-0001-7690-1946

Author 2
- Antonio Gamba, PhD candidate
- Department of Urban and Environment Engineering (UEE), Liege University, Liège, Belgium.
- https://orcid.org/0000-0001-5937-577X

Author 3
- Xu Dai, BEng, MSc, PhD
- School of Engineering, BRE Centre for Fire Safety Engineering, The University of Edinburgh, Edinburgh, United Kingdom
- https://orcid.org/0000-0002-9617-7681

Author 4
- Stephen Welch, MA (Cantab), MSc, PhD
- School of Engineering, BRE Centre for Fire Safety Engineering, The University of Edinburgh, Edinburgh, United Kingdom
- https://orcid.org/0000-0002-9060-0223

Author 5
- Olivier Vassart, Professor
- ArcelorMittal Steligence®, Esch/Alzette, Luxembourg
- https://orcid.org/0000-0001-5272-173X

Author 6
- Jean-Marc Franssen, Professor
- Department of Urban and Environment Engineering (UEE), Liege University, Liège, Belgium.
- https://orcid.org/0000-0003-2655-5648

Full contact details of corresponding author.

Marion Charlier

Research Engineer

marion.charlier@arcelormittal.com

ArcelorMittal Global R&D, Esch/Alzette, Luxembourg

Abstract (150 – 200 words)

The response of structures exposed to fire is highly dependent on the type of fire that occurs, which is in turn very dependent on the compartment geometry. In the frame of the European RFCS TRAFIR project, CFD simulations using FDS software were carried out to analyse the influence of compartment geometry and the interaction with representative fuel loads to explore the conditions leading to the development of a travelling fire. The influence observed of ceiling height, crib spacing, and opening geometry in controlling spread rates tend to confirm the possibility to predict the occurrence, or not, of travelling fire. The results of one CFD analysis are then used to perform a nonlinear thermomechanical analysis of a steel structure with SAFIR® software. Indeed, it is possible to use the radiative intensities and gas temperatures obtained with CFD to calculate with FEM the temperatures in structural elements located in the compartment, and to evaluate the structural behaviour of a frame made of these elements. This paper therefore highlights the effect of building design specifications on the temperature development and on the resulting mechanical behaviour of a steel structure that considers comprehensively the travelling nature of the fire.

Keywords chosen from ICE Publishing list
Fire engineering
Computational mechanics
Steel structures

List of notations (examples below)

RFCS	Acronym for “Research Fund for Coal and Steel”
CFD	Computational Fluid Dynamics
FEM	Finite Element Method
$D^*/\delta x$	non-dimensional parameter to assess the quality of the mesh in FDS
VENT	Used to prescribe planes adjacent to obstructions or external walls in FDS
HRRPUA	Heat Release Rate per Unit Area (kW/m^2)
CPU	Central Processing Unit

Introduction

Small compartment fires behave in a relatively well understood manner, usually defined as post-flashover fires, where the temperatures within the compartment are considered to be uniform. Yet, fires in large compartments do not always reach a post-flashover fire state and there is instead a more localised fire that may travel within the compartment. More recently, the "travelling fire" terminology (Stern-Gottfried and Rein, 2012; Dai et al., 2020) has been used to define fires burning locally and moving across entire floor plates over a period of time. Several studies (Horová et al., 2013; Rush et al., 2015; Hidalgo et al., 2017) have been presented about the behaviour of a structure when it is subjected to a travelling fire. These experimental campaigns provide first insights regarding the parameters influencing fire spread, such as heat release rate density and wood moisture content. Furthermore, in 2005, an experimental programme (Thomas et al., 2005) was set in a deep enclosure and the main conclusion was that fires in deep compartments are strongly affected by the ventilation. Nevertheless, no proper information or scientific knowledge has been established yet on the configurations that can lead to the development of travelling fires (Dai et al., 2017). In the frame of the TRAFIR project, several CFD numerical simulations were made to identify the parameters that may lead to a travelling fire. This paper presents some of these simulations and explains how the CFD results can be used to perform a numerical analysis of the temperature development and resulting mechanical behaviour of a steel structure that considers comprehensively the travelling nature of the fire.

2. THE SETUP OF CFD SIMULATIONS AND ITS CORRESPONDING ASSUMPTIONS

2.1 Computational domain

The Fire Dynamics Simulator (FDS, version 6.7.0) is adopted as the numerical simulation tool. The cell size used in the FDS models depends highly on the situation that is modelled and on the purpose of the simulation. For simulations involving buoyant plumes, the FDS User's Guide (McGrattan et al., 2017) defines a non-dimensional parameter to assess the quality of the mesh: $D^*/\delta x$. In all the hereafter described simulations, cell size of 0.25m x 0.25m x 0.25m was considered. These values were not based on a sensitivity analysis but on existing analyses

representing fire dynamics in large enclosures. Indeed, the FDS Validation Guide contains a table of the values of D*/δx used in the simulation of the validation experiments which were used as guidance. Extra cells have been defined outside the compartment boundaries in order to consider the coupling to the external environment.

2.2 Fire load

The fire load is supposed to be made of discrete wood cribs. No detailed representation of a wood crib (i.e. involving alternation of sticks and air gaps) was used but a simpler approach was adopted, using 1m^3 solid cubes. This approach is based on the work done by (Degler et al., 2015) and (Horová, 2015). It was also used by (Dai et al., 2019); each box was prescribed with experimental measured mass loss and the experimental thermal field development was successfully reconstructed. The overall heat release rate was used as input to VENTs, with each VENT representing a wood crib burning surface (the VENT group is used to prescribe planes adjacent to obstructions or external walls). The wood constituting the cubes is assumed to be red oak type with the following chemical composition: $C_{3.4}H_{5.78}O_{2.448}N_{0.0034}$ and a soot yield of 0.0015 g/g. These values are adopted from the Society of Fire Protection Engineers Handbook (2002). The properties of the modelled wood are: conductivity 0.1 W/m/K, specific heat 1.3 kJ/kg/K, emissivity 0.9 and density 400 kg/m^3. The predefined HRRPUA curve considered come from Degler et al.: it was first obtained numerically using the complex pyrolysis model in FDS then validated by comparison with pallet HRRPUA curves obtained experimentally. The HRRPUA curve has a peak at 480 kW/m^2 and lasts for 33 minutes in total. The Heat Release Rate curve resulting from one cube burning is depicted on Fig. 1.

2.3 Fire spread and heat release rate

Planar devices were placed on each face of the cribs (except on the face in contact with the floor) to measure the temperatures on the solid surfaces. In FDS, quantitative results can be obtained through the use of devices, evaluated using cell centered or face centered values of the cell the device is located in. Devices on solid surfaces allow prescribing a solid phase quantity, and they can be coupled with a spatial statistics option (in which case the output quantity is not associated with just a single point on the surface). The special statistics option MAX was used, and caused FDS to write out the maximum value of the surface temperature

over the cells that are included in the specified bounded volume. If the surface temperature reaches 300°C on at least one face of the volume, then the five surfaces are set to start burning following the prescribed HRRPUA (Heat Release Rate Per Unit Area) curve. This temperature of ignition was arbitrarily set equal to 300°C, which is a reasonable approximation of ignition temperature for certain cellulosic materials (Society of Fire Protection Engineers Handbook, 2002). Before reaching ignition, the face heating is computed by FDS considering radiative and convective heat transfers from the surroundings. When ignition occurs, the HRPRUA curve starts as prescribed, with no further consideration of the radiative and convective exchanges with the surroundings: FDS generates combustible gases that, if entirely burnt, will result in the prescribed heat release rate. Nevertheless, if insufficient oxygen is available, some gas may be left unburnt and the released heat will therefore be less than the one prescribed.

2.4 Boundary conditions

The openings represented in the models are present from the beginning of the fire. Walls and ceiling are made of 25 cm thick concrete (conductivity 2.4 W/m/K, specific heat 1 kJ/kg/K, density 2400 kg/m^3). In all of the compartments presented in this paper, openings are present on both walls along the X axis, and centred. For the sake of clarity, the X and Y axis mentioned hereafter correspond, respectively, to the horizontal and the vertical axis of plan views of the compartments.

2.5 Radiation

The number of radiation angles was set to 100, i.e. the value prescribed by default in FDS. The flame temperature (as opposed to the average cell temperature) is not reliably calculated in a large-scale fire simulation because the flame sheet is not well-resolved on a relatively coarse numerical grid (McGrattan et al., 2017). This implies that the source term in the radiation transport equation cannot be reliably calculated. A practical alternative to this limitation is to prescribe the radiative fraction, which specifies explicitly the fraction of the total combustion energy that is released in the form of thermal radiation. The FDS default value of radiative fraction, 35%, was not modified and this constitutes a basic assumption of the presented model.

3. MODEL OF DIFFERENT CONFIGURATIONS OF LARGE COMPARTMENTS: RESULTS AND INFLUENCES

Different typologies of large compartments were modelled: the conditions supporting travelling fire development are explored by varying some of the fundamental inputs to the model, i.e. ceiling height, opening size, fuel load density and compartment layout. Two series of configurations are investigated, in which series 1 relates to a deep rectangular compartment and series 2 relates to a large square compartment. Table 1. summarizes the different configurations analysed in the frame of this paper.

Table 1. Different configurations of large compartments

Config.	Compartment dimensions X,Y,Z (m)	CFD Domain dimensions X,Y,Z (m)	Opening size (m)	Opening factor $m^{1/2}$	Separation between the cribs (m)	Fire load (MJ/m^2)
1.a	50 x 10 x 4	60 x 12 x 6	45 x 3.5	0.40	1	550
1.b	50 x 10 x 4	60 x 12 x 6	20 x 3.25	0.16	1	550
2.a	20 x 20 x 8	24 x 24 x 9	16 x 6.75	0.39	2	270
2.b	20 x 20 x 3.5	24 x 24 x 4	16 x 2.25	0.10	2	270

3.1 Deep rectangular compartment – 1D spread

In configuration 1, a 50m x 10m x 4m compartment is defined in a model domain of 60m x 12m x 5m. The openings extend vertically from 0.25m above floor level. In both configurations (1.a and 1.b) the fire starts by the ignition of the wood crib placed at the left-end of the compartment, at mid-width (see Fig. 2). Figures 3,4,5 and 7 depict iso-lines representing the fire front edge locations at different times. According to Fig. 3, in configuration 1.a the fire spreads slowly at the beginning (0m – 15m), then faster (15m – 50m) when the effects of pre-heating by radiation from the hot layer become more significant. Specifically, at beginning of the fire (0 – 20 minutes), the pattern of the burning area indicates a t^2 development, but the acceleration is soon damped with the remaining spread being closer to a steady rate of increase along the length of the compartment. Steady spread can be expected when the process is being driven primarily by local crib-to-crib spread and where the effects of preheating from the hot layer to cribs ahead of the front is relatively minor, and does not significantly increase with time. Also, the fire spread front edge has a clear time lag when it is in the area near the openings, as depicted on Fig. 3 around y=0m and y=10m. This may be due to the fact that in those areas the

pyrolysis is moderated by exposure to the adjacent cold ambient air and the main combustion zone at the diffusion interface in the gas phase is not moving ahead of the pyrolysis zone. As shown in Fig. 3 and Fig. 4, the fire spreads much faster overall under configuration 1.b compared with configuration 1.a. Indeed, configuration 1.b requires 52 minutes to spread over the whole compartment compared to 90 minutes for configuration 1.a. This can be explained by more energy leaving the compartment through the larger openings of configuration 1.a. Compared with configuration 1.a, the compartment of configuration 1.b is more likely to increase the fire spread rate, due to greater retained heat but also due to the burning zone seeking oxygen towards the openings (0m – 10m). For both configurations, the prescribed Heat Release Rate matches the computed value obtained from the code, implying no significantly ventilation controlled situations.

Some interesting differences are also apparent in the instantaneous fire spread rate evolution. The speed at the horizontal centreline, versus X location, is directly represented in Fig. 5. The values are determined from the straight-line distance between two ignited wood crib centres (mm) divided by the time for the second wood crib being ignited (s) and for each of these values, the depicted relative X location corresponds to the mid-distance between two ignited wood cribs. Thus, higher velocity regions of the chart represent rapid transitions between cribs, but are of relatively short duration. In configuration 1.b when the fire has passed the opening (10m – 20m), more oxygen is available to sustain more vigorous combustion, and compensating to some extent for the reduction in retained heat. This may be part of the reason that the fire spread rate is higher in this region, compared with the region from 0m – 10m. Then the fire spread rate decreases from 30m – 35m as access to oxygen diminishes towards end of opening. In configuration 1.b, at the region of 35m – 50m, the fire spread rate increases again, due to heat retention in the more enclosed region, though much of the gas-phase combustion may still be located near the opening at around 35m. Moreover, as shown in Fig. 5, the fire spread rate in configuration 1.b is at times significantly higher than the one in configuration 1.a. Overall, compared to the more open configuration 1.a, the fire travel format in configuration 1.b is less steady, being strongly influenced by phenomena associated with the smaller openings.

147 For all wood cribs of configuration 1.a, the triggered surface is the one facing the previous cribs,
148 revealing that the radiation of the previous burning wood crib might play the major role in the fire
149 spread. For configuration 1.b, it is also the case for the wood cribs situated at the left end of the
150 compartment and the right end of the openings. However, for the wood cribs at the left end of
151 the openings and at the right end of the compartment, the triggered surface is the one facing the
152 ceiling due to the radiation from the hot smoke layer. This implies that the presence of openings
153 changes the fire spread mechanism, as has been observed experimentally (Gupta et al. 2020).
154 For both configurations, the Heat Release Rate computed by FDS coincides with the imposed
155 Heat Release Rate (prescribed through HRRPUA curves), which confirms that there is no
156 unburnt gaseous fuel.
157
158 ***3.2 Square compartment – 2D spread***
159 In configurations 2.a and 2.b, the compartment dimensions are respectively 20m x 20m x 8m
160 and 20m x 20m x 3.5m and the model domains respectively 21m x 21m x 9m and 24m x 24m x
161 4m. The openings are placed 0.25m above floor level. The fire starts by the ignition of the wood
162 crib placed at the centre of the compartment and the fire load consists of $1m^3$ wood cribs
163 spaced 2m away from each other. This fuel density was chosen to represent the rate of heat
164 release density of an office building prescribed by the Annex E of Eurocode 1 (EN1991-1-2,
165 2002), which is 250 kW/m^2. When compared with configurations 1, the results indicate generally
166 slower spread rates, which is consistent with the greater crib spacing. Also, a 2D spread is
167 observed in both cases, but with a slightly slower spread at the openings side for configuration
168 2.a where less heat is retained, as depicted in Fig. 6.a. In configuration 2.b the fire spread
169 accelerates more rapidly, taking 28 minutes to spread over the entire floor versus 45 minutes in
170 configuration 2.a. This difference is suggested to result mainly from lowering the ceiling height,
171 due to the stronger coupling between the hot gases and the pyrolyzing cubes. The change of
172 opening factor also impacts on the ventilation airflows at the openings, and the more regular
173 spread depicted on Fig. 6.b is a net result of the enhanced heat transfer with the lower ceiling,
174 together with changes in burning behaviour related to ventilation differences and the reduced
175 overall duration of spread.
176

4. LINKING CFD AND FEM: RESPONSE OF A STEEL STRUCTURE TO THE TRAVELLING FIRE CHARACTERISTICS

4.1 Modelling strategy

The CFD analyses are performed with a model of the compartment that does not necessarily contain the structural elements (Welch et al., 2008; Tondini et al., 2016). Structural elements must be present in the CFD model if they form a boundary of the fire compartment (walls and ceiling slab) or if they significantly influence the mass flow or the radiative flow in the compartment (deep concrete beams, wide columns, shear walls…). If the structure is made of linear steel members, it is likely that the characteristic size in the transverse direction of the steel elements is small with respect to the characteristic length of the compartment, which can justify the absence of these elements in the CFD domain. A dedicated version of FDS 6 has been written where the sole modification is the creation by FDS of a new file in which particular results are written to be used by the subsequent structural analysis by SAFIR (Franssen and Gernay, 2017). The coupled code has previously been verified in the frame of to two practical examples: a steel rack system next to a pool fire (Tondini et al., 2012) and an open car park (Tondini et al., 2016)". The results are:

- gas temperature, used for the convective heat transfer to the structural elements;
- coefficient of convection, depends on the gas velocity. NB – SAFIR does not currently use this coefficient; it uses a constant value, for example 35 W/m²K, for simplicity;
- radiation intensity in several directions. These intensities have been preferred to the impinging flux or the adiabatic surface temperature for different orientations, because these latter quantities both result from an integral on a surface and the information about the direction of the impinging intensities considered in these integrals is lost, with the consequence that concave sections cannot be considered appropriately.

In order to reduce the size of this transfer file, the time steps, the spatial steps in the 3 directions, as well as the limits of the domain covered in the file, do not necessarily coincide with the respective values of the CFD analysis. Linear interpolations are used by FDS between its internal results to write the file, and linear interpolations are performed by SAFIR when reading the file to compute the relevant values at the requested positions in time and in space. Based on the data found in the transfer file, a series of 2D transient thermal analyses are performed along

the structural members and the results are stored in appropriate files. As these 2D temperature distributions will be used subsequently to represent the temperature in beam finite elements, a temperature distribution is calculated for each longitudinal point of integration of each beam finite element; SAFIR uses 2 or 3 points of Gauss along the beam elements. In these 2D thermal analyses, the impinging flux is computed for each boundary (in the sense of finite element discretisation) of the section, depending on its orientation. As an approximation, the position of the boundaries of the section in the fire compartment is the same for all boundaries of a section (at the position of the node line of the beam finite element, based on the assumption that half of the characteristic length of the section is small with respect to the size of the compartment). For the boundaries on concave parts of the section, impinging radiative intensities from certain direction are discarded if there is an obstruction by other parts of the section. Mutual radiation between different boundaries of the section in the concave regions is not considered. Generally, in the CFD model, the dimensions of a rectangular compartment correspond to the clear distances between opposite walls. However, in the FE model, a slab is generally modelled in correspondence to its centreline. Thus, the slab would fall outside the CFD domain, and assumptions have to be made to determine thermal information at the slab centreline.

4.2 Example

4.2.1 Configuration of the compartment

In this example, a compartment similar to the one depicted in Fig. 2, i.e. a 51m x 9m x 4m compartment with 20m x 3.25m opening size, is considered. While the compartment geometry is similar to the one of configuration 1.b, there is a difference in the rate of heat release density. Considering the maximum value of the rate of heat release curve of a cube and a floor averaged distribution, the solid cribs are in this case spaced 2m away from each other to represent the rate of heat release density of an office building, which is 250 kW/m^2 (EN1991-1-2, 2002). As for previous configurations, the Fig. 7 depicts isolines representing the positions of the fire front in the compartment, at different times. Though the initial spread of the fire is quite similar to that seen for configuration 1.a, the subsequent progress is slower by about a factor of two until the end of the fire, a trend which can be attributed to the greater spacing between the cribs, which results in the fire taking significantly longer to spread between the individual fuel parcels, as well

as the reduction in the peak burning rate per unit floor area (i.e. 245 kW/m^2 versus 600 kW/m^2 for 1.a). Apart from the spread rate the behaviours otherwise appear to be broadly comparable.

4.2.2 Steel structure

To illustrate the capabilities of the CFD-FEM coupling, the steel framed structure made of hot rolled steel profiles shown on Fig.8 is supposed to be present in the compartment described above. In the FE analysis (in SAFIR, each column is discretized into 4 BEAM elements and each beam of the frame is discretized into 6 BEAM elements. Two points of Gauss are defined along the BEAM elements.. For the thermal analyses, the emissivity of steel was set to 0.7 and the convection coefficient to 35 W/m²K, following EN 1991-1-2. The number of directions in which the radiation intensities are computed is set to 72, which is recommended as minimum when analysing structural members that entails shadow effects. For the subsequent mechanical analysis, the frame located at mid-width of the compartment (spanning along X axis) is considered. The steel sections of the beams are IPE 400 while those of the columns are HE 200 A, in steel grade S275. The columns are completely fixed at the base, while one direction has been fixed at the top to avoid out of plane displacements. A uniformly distributed loading of 6,5 kN/m is applied on the beams, corresponding to 142 kg/m².

4.2.3 Results

Fig. 9.a shows one result of the thermal analysis performed by SAFIR: the isotherms after 41 minutes in the IPE400 beam in the middle of the first span (point A in Fig. 8). A clear difference is observed between the lower flange and the upper flange, the latter being exposed to fire only on 3 sides. A gradient can also be observed in the flanges from right (toward the centre of the compartment) to left (toward the wall). Also, the lower part of the web is somehow protected by the lower flange from the radiation intensities that come mainly from the bottom right direction (i.e. the ground in the compartment). Fig. 9.b shows the evolution of the temperature in the centre of the section in the central beam (from B to F) after 67 and 92 minutes. The offset between the plots reflects the spread of the fire in the compartment. At 67 and 92 minutes, the fire front is situated at X = 21 metres and X = 32 metres, with a fire thickness of approximately 6 meters and 8 meters, respectively. The steel temperature peaks are computed at X = 13 metres

and X = 24 metres, i.e. just after the fire passed. Fig. 10.a shows the node which is considered for plotting the evaluation of the steel temperature along the column height (the central column placed below point B in Fig. 8), which is shown in Fig. 10.b for three times: 90 minutes (when the column is within in the fire zone), 100 minutes (when the fire zone starts to leave the column) and 110 minutes This figure translates a thermal gradient along the height of the compartment with maximum temperatures (steel temperatures are considered at the locations of the Gauss Nodes in the column) and, as Fig. 9.b, reflects the spread of the fire in the compartment.

The temperatures computed in the sections of the 3D beam finite elements that form the structure are taken into account in a geometrically transient and materially nonlinear structural analysis performed with SAFIR. Many different results can be obtained from this type of analysis, such as the evolution of axial forces and bending moments in the elements, the stresses in the elements, the displacements of the nodes and finally, the fire resistance time and the failure mode (or the absence of failure). The evolution of the vertical displacement at the top of the five columns from the central frame is represented on Fig. 11. As the structure does not collapse, the vertical displacement is essentially elastic and is therefore a result of thermal elongation. The travelling nature of the fire is highlighted by the time shift of the thermal elongation in the columns B to F.

5. Discussions and further improvements

The sample cases presented illustrate the potential value of CFD for generating and analysing fire dynamic conditions which influence the likelihood of fire spread. It is important to note that these are numerical examples and not validation studies. Thus there are important provisos on the interpretation of the results. Further work would be required to quantify any deviations arising due to numerical effects.

Also, the methodology used for the representation of burning fuel has some limitations. Before a cell reaches the ignition temperature, its heating is computed while considering heat exchanges with the environment. But as soon as the ignition temperature is met, FDS represents the fire by

297 releasing volatile combustibles which, if all are burnt, results in the prescribed HRR curve. This
298 is done without considering the evolution of heat exchange with the environment. Moreover, the
299 uniform cubic shape of the obstruction prevents air flow through the object. Nevertheless, it was
300 concluded that this approach can yield a good representation of an isolated burning wood crib in
301 comparison with hand calculations of the upper and mean value of the mass loss rate (Degler J
302 and Eliasson A, 2015).
303
304 Furthermore, the details of glazing failure have been ignored at this stage, and more realistic
305 compartment geometries and boundary materials should also be considered. Crib burning rates
306 are affected by the proximity to the compartment boundaries but the simplified representation
307 adopted does not admit the known enhancement of the burning rate arising from the additional
308 heat transfer contribution in a corner fire.
309
310 Moreover, having demonstrated the value of the methodology, further systematic use of
311 numerical simulations will be undertaken to perform more comprehensive parametrical
312 analyses. The calibration of these simulations will also benefit from experimental tests from the
313 literature and those performed in the frame of the TRAFIR project. It will then be possible to
314 determine with more confidence the conditions in which a travelling fire may develop, or not,
315 and therefore inform on appropriate fire scenarios to be considered. Experimental campaign
316 launched in the frame of the same project and further CFD analyses are described in (Nadjai et
317 al. (2020); Charlier et al. (2020)).
318
319 Concerning SAFIR, parallelisation of the code which is currently under way, which will reduce
320 the CPU time requested for the large number of 2D thermal analyses performed in the sections.
321
322 **6. Conclusions**
323 Using the Fire Dynamics Simulator (FDS), different geometrical arrangements were modelled in
324 terms of compartment layout, opening size and ceiling height. A fire load composed of wood
325 cribs has been considered using discrete volumes arranged on regular grids, and a temperature
326 criterion on the volume surfaces was used to trigger the start of a predefined heat release curve.

Some useful quantitative measures of fire behaviour were extracted from the CFD results, in particular the fire spread rates, facilitating analysis of characteristic behaviours. It was possible to interpret all the observed trends in terms of fundamental principles of fire dynamics. The method for study via this kind of representative simulations is built on several explicit assumptions, but nevertheless permits a first assessment of the conditions required for fire spread and provides an indication of some of the influential parameters and likely sensitivities. In particular, for a given fire load and compartment dimensions, modifying the ventilation conditions (i.e. the opening factor) showed a significant influence on the fire behaviour, consistently with experimental observations (Gupta *et al*. 2020). In the present paper, the studied configurations lead to travelling fire, without encountering ventilation controlled stages, but other ventilation conditions (i.e. reduced openings) could obviously lead to such situations. The implications of such design choices should therefore be investigated to assess the proper fire scenarios to be considered.

Further, by considering the detailed results of the CFD analysis in a nonlinear thermomechanical analysis of a structure located in the fire compartment, the coupling of the structural response to the travelling fire characteristics has been demonstrated. In the presented configurations, such methodology appeared adequate to properly translate the thermal effects linked to the travelling nature of a fire on steel frames made of hot rolled profiles (as observed through the thermal gradient within the sections and offset of the temperature versus time plots).

Acknowledgements

This work was carried out in the frame of the RFCS TRAFIR project with funding from the European Commission (grant N°754198). Partners are ArcelorMittal Belval & Differdange, Liège University, the University of Edinburgh, RISE Research Institutes of Sweden and the University of Ulster.

References

355 Charlier M, Vassart O, Dai X et al. (2020) A simplified representation of travelling fire
356 development in large compartment using CFD analyses. Accepted for the 11th Intl. Conf. on
357 Structures in Fire, 2020.
358
359 Dai X, Welch S and Usmani A (2017) A critical review of 'travelling fire' scenarios for
360 performance-based structural engineering. Fire Safety Journal 91: 568-578.
361
362 Dai X, Welch S, Rush D et al. (2019) Characterising natural fires in large compartments –
363 Revisiting an early travelling fire test (BST/FRS 1993) with CFD. Proceedings 15th International
364 Interflam Conference, London, UK.
365 Dai X, Welch S, Vassart O et al. (2020) An extended travelling fire method framework for
366 performance-based structural design. Fire and Materials 44: 437–457.
367
368 Degler J and Eliasson A (2015) A Priori Modeling of the Tisova Fire Test in FDS, Bachelor's
369 Thesis, Luleå University of Technology, SE.
370
371 Degler J, Eliasson A, Anderson A et al. (2015) A-priori modelling of the Tisova fire test as input
372 to the experimental work. Proceedings 1rst International Conference on Struct. Safety under
373 Fire & Blast, Glasgow, UK.
374
375 EN1991-1-2 (2002). Eurocode 1: Actions on structures - Part 1-2: General actions-Actions on
376 structures exposed to fire. CEN, Brussels.
377
378 Franssen JM and Gernay T (2017) Modeling structures in fire with SAFIR®: theoretical
379 background and capabilities. Journal of Structural Fire Engineering 8: 300-323.
380
381 Gupta V, Hidalgo JP, Cowlard A, et al. (2020) Ventilation effects on the thermal characteristics
382 of fire spread modes in open-plan compartment fires. Fire Safety Science 13 (in press)
383

Hidalgo JP, Cowlard A, Abecassis-Empis C et al. (2017) An experimental study of full-scale open floor plan enclosure fires. Fire Safety Journal 89: 22-40.

Horová K (2015) Modelling of Fire Spread in Structural Fire Engineering. PhD thesis, Czech Technical University in Prague.

Horová K, Jána T and Wald F (2013) Temperature heterogeneity during travelling fire on experimental building. Advances in Engineering Software 62-63: 119-130.

McGrattan K, Hostikka S, McDermott R et al. (2017) Fire Dynamics Simulator User's Guide, Sixth Edit. National Institute of Standards and Technology (NIST).

Nadjai A, Alam N, Charlier M et al. (2020) Travelling fire in full scale experimental building subjected to different ventilation conditions. Accepted for the 11th Intl. Conf. on Structures in Fire, 2020.

Rush D, Lange D, Maclean J et al. (2015) Effects of a Travelling Fire on a Concrete Column - Tisova Fire Test. Proceedings of the 2015 ASFE Conference.

Society of Fire Protection Engineers Handbook (2002) Fire Protection Engineering, Third Edition, National Fire Protection Association, USA.

Stern-Gottfried J and Rein G (2012) Travelling fires for structural design - Part I: Literature review. Fire Safety Journal 54: 74-85.

Thomas I, Moinuddin K, Bennetts I (2005) Fire development in deep enclosure. Fire Safety Science 8: 1277-1288.

Tondini, N., Vassart, O. Franssen, J.-M. (2012) Development of an interface between CFD and FE software. Proceedings of the 7th International Conference on Structures in Fire M. Fontana, A. Frangi, M. Knobloch, Switzerland.

Tondini N, Morbioli A, Vassart O et al. (2016) An integrated modelling strategy between a CFD and an FE software: Methodology and application to compartment fires. Journal of Structural Fire Engineering 7 Issue 3: 217-233.

Welch S, Miles S, Kumar S et al. (2008) FIRESTRUC – Integrating advanced three-dimensional modelling methodologies for predicting thermo-mechanical behaviour of steel and composite structures subjected to natural fires. Fire Safety Science 9: 1315-1326.

Figure captions (images as individual files separate to your MS Word text file).

Figure 1. Heat release rate of one burning cube
Figure 2. Model of configuration 1.b
Figure 3. Fire spread time vs. compartment location, under configuration 1.a
Figure 4. Fire spread time vs. compartment location, under configuration 1.b
Figure 5. Fire spread rate vs. compartment location, under configurations 1.a and 1.b
Figure 6. Fire spread time vs. compartment location under a) configuration 2.a; b) configuration 2.b
Figure 7. Fire spread time vs. compartment location, under configuration to illustrate the capabilities of the CFD-FEM coupling
Figure 8. Steel structure in the compartment and solid cribs
Figure 9. Steel temperatures in beams. a) Isotherms after 41 minutes at A; b) Evolution along central beam B-F
Figure 10. a) Location of the node considered for b) the evaluation of the steel temperature along the height of the central column
Figure 11. Evolution of the elongation of the columns in the central frame as a function of time

Fig. 1

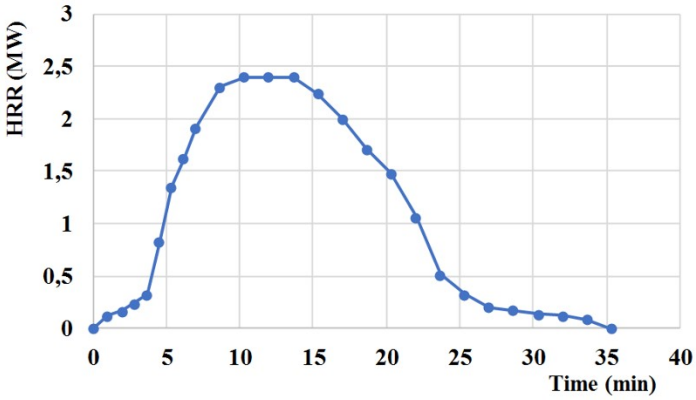

Fig. 2

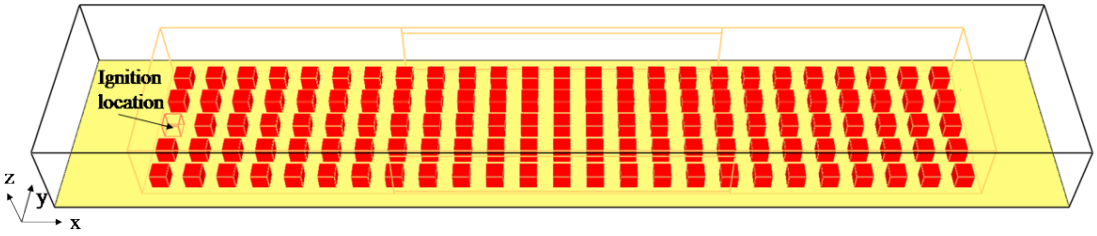

Fig. 3

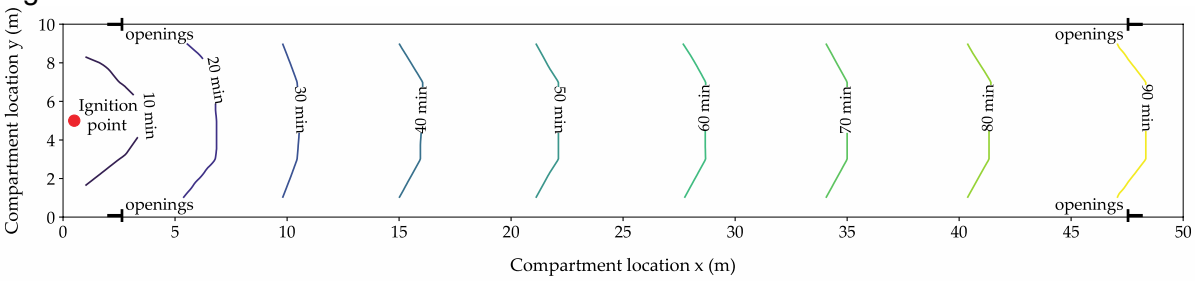

Fig. 4

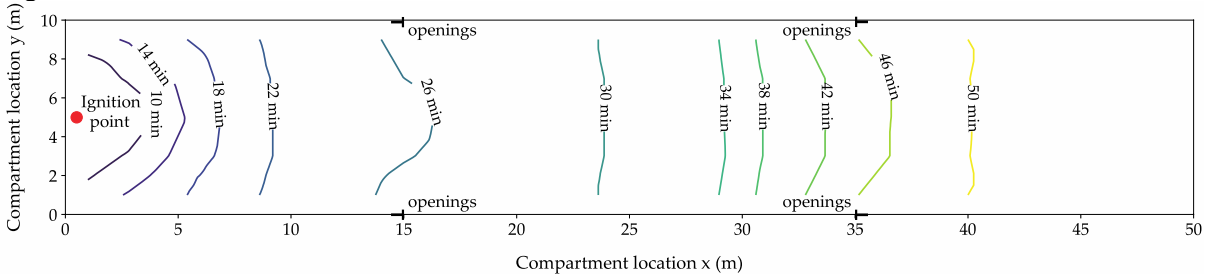

Fig. 5

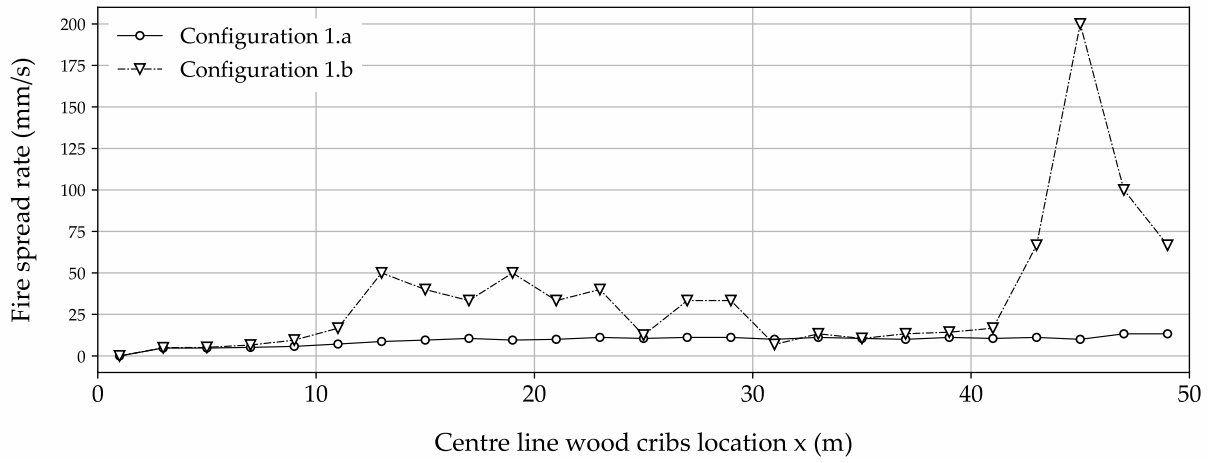

Fig. 6

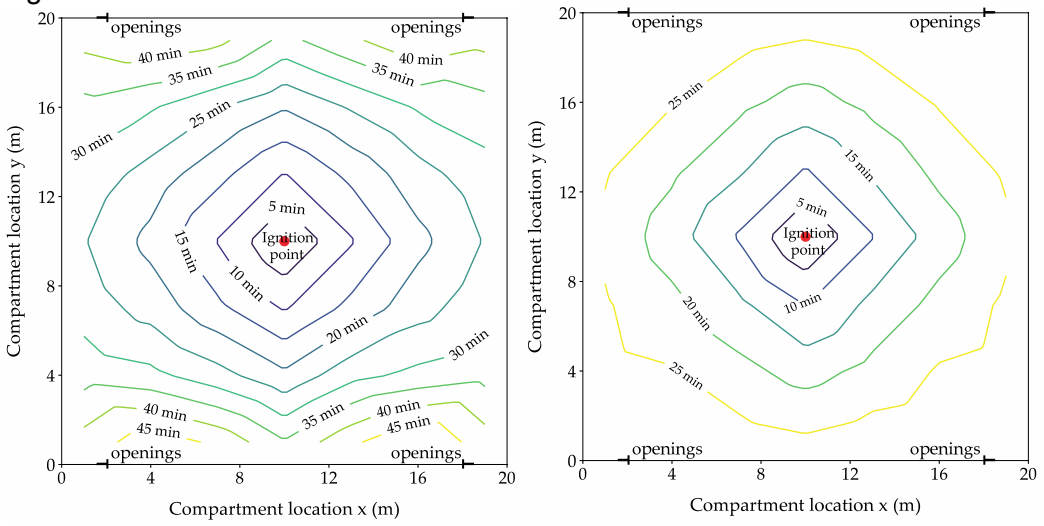

Fig. 7

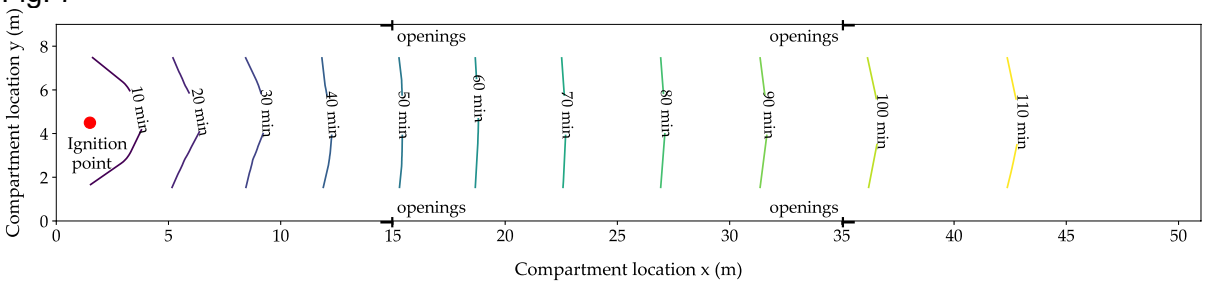

Fig. 8

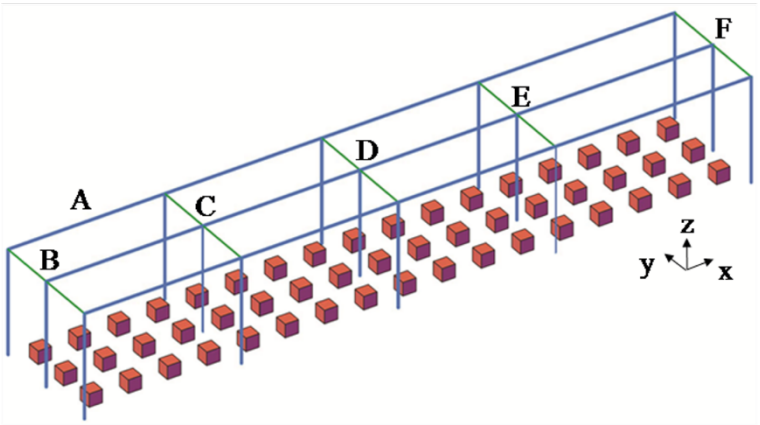

Fig. 9

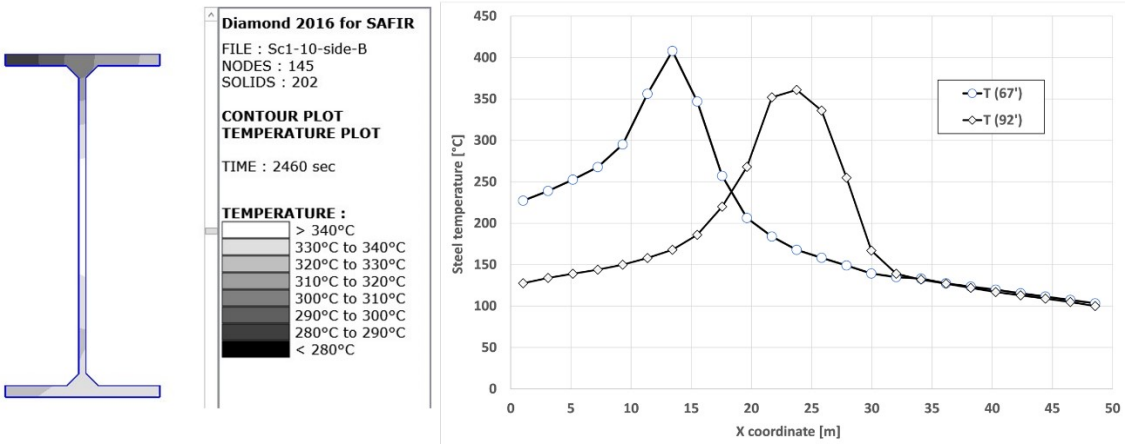

Fig. 10

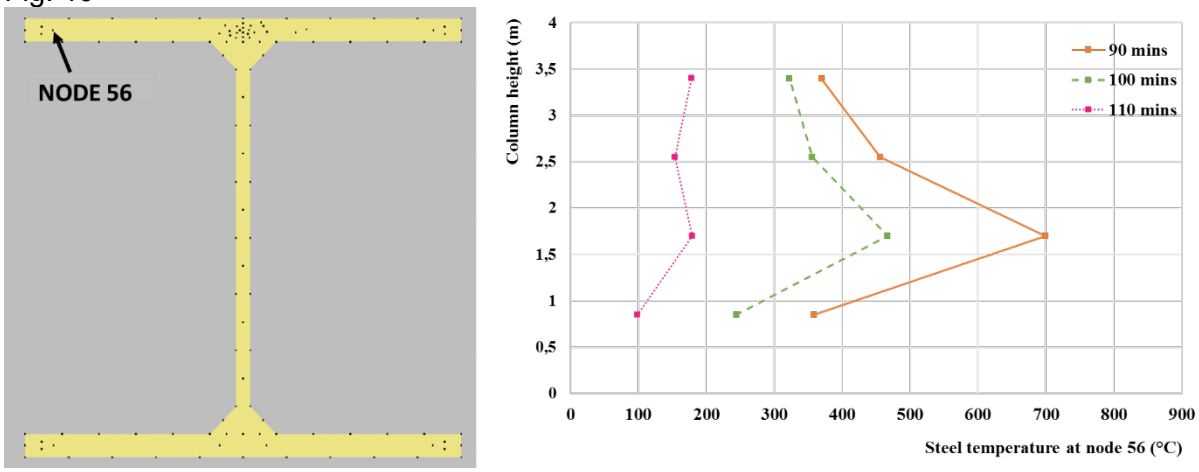

Fig. 11

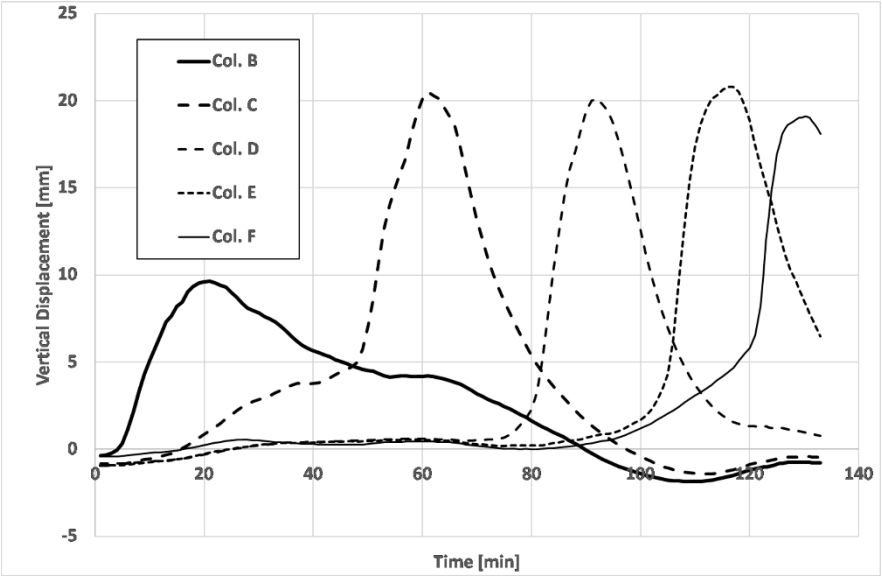
Col. B
Col. C
Col. D
Col. E
Col. F
Vertical Displacement [mm]
Time [min]
25
20
15
10
5
0
-5
0
20
40
60
80
100
120
140

479
480
481